Heliyon 9 (2023) e16310

Contents lists available at ScienceDirect

Heliyon

journal homepage: www.cell.com/heliyon

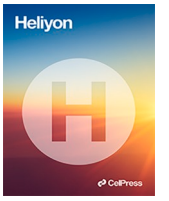

Research article

Radiogenic heat production estimation towards sustainable energy drive in northeastern Nigeria

Abu bakar Yusuf [a,b], Hwee San Lim [a,*], Ismail Ahmad Abir [a]

[a] Geophysics Section, School of Physics, Universiti Sains Malaysia, 11800, Penang, Malaysia
[b] Department of Geology, Faculty of Science, Gombe State University, P.M.B. 127, Gombe, Nigeria

ARTICLE INFO

Keywords:
Gamma ray
Spectrometry
Radiometric
RHP
Gongola basin

ABSTRACT

An estimate of the radiogenic heat production (RHP) across the different petrologic units of northeastern, Nigeria was previously not performed. Hence, their geothermal potentials are not widely known. However, an airborne radiometric data of equivalent uranium, (eU), equivalent thorium (eTh,) and percentage potassium (% K) acquired by Nigerian geological survey agency (NGSA) in the year 2009 was deployed in the evaluation of the RHP across the major petrologic outcrops of northeastern, Nigeria. The objective of this study is to estimate the quantity of RHP across the 13 petrologic units of the northeastern Nigerian terrain via the use of an empirical equation ($RHP = \rho(0.0952\,C_u + 0.0256\,C_{Th} + 0.0348\,C_k)$). The petrologic units studied are; medium-coarse grained biotite-hornblende granites (*OGe*), porphyritic biotite-hornblende granites (*OGp*), banded gneiss (*bG*), charnokytes (*Ch*), ignimbrites (*JYG*), migmatites-gneiss (*MG*), basalts (*bb*), Gombe sandstones (*GS*), Pindiga Formation (*PS*), Yolde Formation (*YL*), Bima sandstones (*BS*), Keri-Keri Formation (*KK*), and alluvium (*AL*). Basic/preliminary processing such as; signal integration, signal validation, and examination of spurious data were applied prior to the RHP computation. The results of the heat production analysis performed show the range of RHP to be from 1.11 $\mu W/m^3$ to 3.35 $\mu W/m^3$ Hence, the maximum heat production value of 3.35 $\mu W/m^3$ was recorded along porphyritic biotite-hornblende granites (*OGp*) rock block, while the least value of 1.11 $\mu W/m^3$ was recorded over alluvium (*AL*) rock outcrops. Furthermore, the spatial distribution of the RHP values over the study location shows a gradual increase from the middle, low heat production (sedimentary zones) to the high heat producing areas (granitic and metamorphic zones) around eastern and western parts. The petrologic units arranged in order of decreasing magnitude of radiogenic heat generation are; *OGp* > *MG* > *OGe/bG* > *bb* > *GS* > *Ch* > *JYG* > *BS* > *PS/YL* > *KK* > *AL*. On a general note, the petrologic units studied were classified as low in terms of geothermal character based on comparison with other previous global RHP studies.

1. Introduction

An airborne radiometric, deals with the measure of radioactive heat emitted from the earth's crustal and upper mantle rock using a spectrometer attached to an air aircraft [1,2]. The spontaneous decay of radioactive elements (mostly of ^{238}U, ^{232}Th, and ^{40}K) found

* Corresponding author.
E-mail address: hslim@usm.my (H.S. Lim).

https://doi.org/10.1016/j.heliyon.2023.e16310
Received 27 December 2022; Received in revised form 11 May 2023; Accepted 12 May 2023
Available online 24 May 2023

within the rock minerals of the crusts results to release of gamma radiation that can be measured using a detector [3,4]. The energy generated through radiogenic process is a major factor being considered for geothermal investigations [4,5]. Hence, the need for its evaluation in global sustainable energy drive. Moreover, an acquired airborne radiometric data usually has a spectral resolution that depends largely on the line spacing of the survey design [6]. The choice of a flight line intervals is a product of a compromise between cost of acquiring the data and the data resolution [6]. Therefore, a higher resolution data requires a higher acquisition cost and vice-versa. The intensity of radiation being emitted in an area depend on the quantity of the naturally occurring radioactive minerals present in the rock [7]. Hence, the geology and tectonics of an area is a significant factor in radiometric exploration. The measured radioactive signals can only emanates from the shallower (few centimeters) parts of the crust, as such, it's unable to measure signals from deeply seated anomalies [3]. Radiometric methods have been widely applied in different case studies across different countries of the world. The studies were performed in order to tackle different problems such as environmental hazards, minerals prospecting, geological mapping [8], radiogenic heat production (RHP) studies [9,10], and [11].

Several efforts were made in the past to study the radioactive mineral composition of the rocks of the northeastern Nigerian geological terrain (comprising of both the sedimentary and the basements parts) especially, the uranium enrichment areas. These include the studies by [12–23]. The above-mentioned studies used the various geological, petrological, and geochemical methods in the study of these areas in terms of radioactive mineral occurrences, origin, and their host structures. RHP studies have been widely

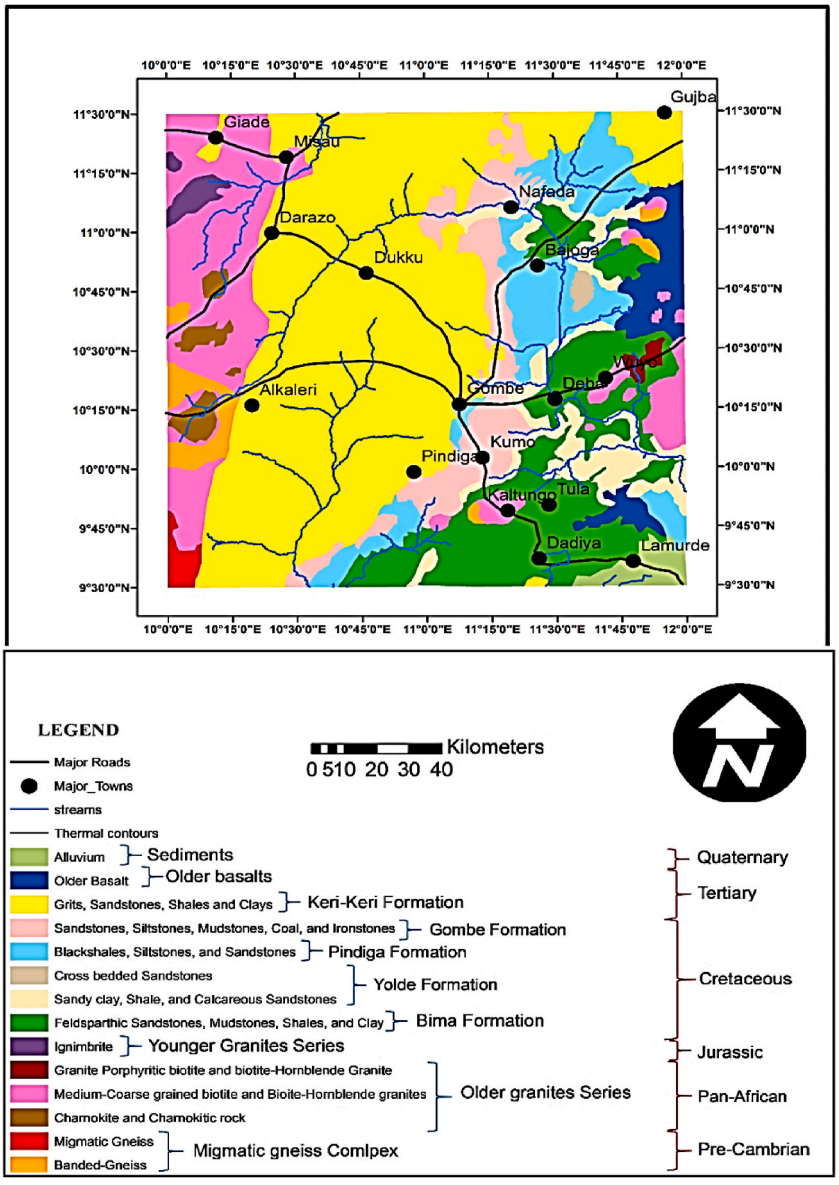

Fig. 1. Geological map of the study area (modified after [27]).

applied in sedimentary, metamorphic, and igneous terrains [10,24,25].

However, RHP studies in northeastern Nigeria is very scanty. The only available geophysical approach to the study of the radioactive mineral occurrence and their tectonic control was the study by [26] who used airborne magnetic and radiometric data to study the uranium enrichments areas as well as their tectonic set-up. The study identified new areas of uranium enrichments that have not been previously known. However, it did not compute (estimates) the amount of RHP that could be generated from this area for possible assessment for further exploration for nuclear energy generation.

Hence, the present study tried to fill the incomplete study gap of estimating the amount of RHP of the several petrologies spanning from the sedimentary, metamorphic, and igneous outcrops of northeastern Nigeria, using a higher resolution airborne radiometric data, which helps in revealing areas of greater heat production for possible exploration in the future.

2. Geological settings

The current study area is geographically located within longitudes 10° 00′ E to 12° 00′ E, and latitudes: 9° 30′ N to 11° 30′ N. The total areal land surface covered by the study area is 49,284 km^2. The area's geomorphological features include; hills, valleys, and a number of stream channels (Fig. 1).

Geologically, the study area is composed of three (3) main group of rocks that includes; the Precambrian basement rocks, the cretaceous to recent sedimentary rocks, and the tertiary volcanics that intruded the pre-existing rocks (Fig. 1) [27]. The crystalline basement rocks outcrops are migmatic gneiss, banded gneiss, charnokytes, ignimbrites, porphyritic biotite - hornblende granites, medium grained biotite - hornblende granites [27]. The cretaceous - recent sedimentary petrologies include: the continental Bima formation, the transitional Yolde formation, the marine Pindiga formation, the continental Gombe formation, Kerri-Kerri formation in addition to the recent alluvium deposits [28]. Other rock outcrops include tertiary older basaltic plugs found at the extreme eastern and south eastern parts of the study area (Fig. 1).

3. Materials and methods

3.1. Aerial gamma ray spectrometry technique

An aerial gamma ray spectrometry (AGRS) simply refers to a procedure applied in measurements of a spectrum energy and radiation intensity over a given area [29]. The procedure involved the use of an aircraft with an attached spectrometer (detector) to fly over a specified survey area. It enables recording of the amount of radiation from the survey area. AGRS received wide application in several countries of the world, such as America, Britain, Canada, Germany, Russia, Sweden, Syria, Iran, Egypt, Nigeria, among many others [29].

The airborne radiometric data set used in this study are; forty-eight (48) half degrees high resolution digital data grids on a scale of 1:100,000. They were acquired by Fugro airborne survey limited, Johannesburg, South Africa from 7th December 2006 to 31st May 2007. It is part of a program aimed at assisting and promoting mineral exploration in Nigeria. A fixed wing aircraft was deployed to the surveyed area. Moreover, during the survey activity, the whole of Nigerian landscape was divided into 10 blocks (A1, A2, B, C, D1, D2, D3, D4, D5, and the Pilot scheme segments, (Fig. 2). The present study area spans over a fragment of blocks, D1, D2, A & C (Fig. 2.)

A GPX 1024/256-channel gamma-ray spectrometer was deployed to measure the amount of radiation over the research area. The sensors arrangement encompasses primary detector used in quantifying the land-sourced gamma radiation and secondary detector which was applied in quantifying the amount of atmospheric radon. The primary detector consists of 3 sensor bundles, with each bundle comprising of 4 crystals of sodium-iodide (NaI), and thallium-activated (Tl) sensors. Each of the sensors has a dimension of 4 by

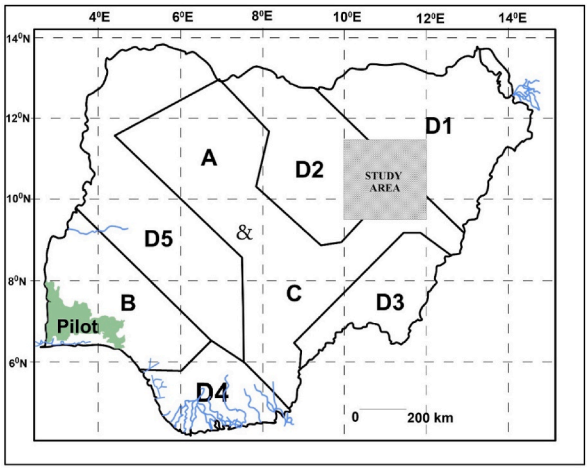

Fig. 2. Map of Nigeria showing various blocks where airborne radiometric data acquisition was performed (modified after [30]).

4 by 16 inches (256 cubic inches). The 4 crystals enclosed in each bundle were placed in close contact with one another. It also has a dimension of 16 by 16 by 4 inches (equivalent to; 16.78 L). The primary sensor has a total volume of 50.341 L. The secondary detector encompasses two crystals of sodium-iodide, thallium-activated (NaI "Tl") sensors of equal measurements (dimension). The volume of the secondary detector is 8.39 L. A heated and thermally stabilized vessel was used to enclose each of the detection bundle. This is to ensure spectral stability of the system [30].

Spectrometer was deployed to acquire the gamma-ray spectrum at an interval of 1 s. The Survey was conducted while the above detector was fixed to an aircraft that flew over the study blocks using a flight trend of 125°.

The other survey parameters used includes; a flight line spacing of 500 m, a flight direction of northwest - southeast, terrain clearance of 80 m, tie line spacing of 2000 m, and a tie-line direction of northeast - southwest. These radiometric data were earlier pre-processed by the company that acquires it before presenting the result in form of data grids for subsequent usage. This was done in order to correct for influences that are non-geological in nature. The pre-processing, and processing activities applied to the acquired data are; Signals merging, examination of missing or spurious data, and data validation among others. The above listed corrections were performed in order to ensure data quality check [5]. Other processing applied are; terrain clearance variation corrections, and general background correction (which is due to non-geologic influences such as; atmospheric radon, cosmic rays etc.).

Hence, out of the total of 48 grids (sheets) used for the present research, a total of 16 sheets were merged to form a composite equivalent uranium concentration map of the study area (Fig. 2) using geosoft software. The other two sets of 16 sheets each for thorium and potassium radio elements were also merged separately forming two separate maps for equivalent thorium, and percentage potassium elements distribution maps respectively. The total count map of the study area portrays the composite effects of *U, Th, and K*. It was produced (formed) via integration of the *eU, eTh, and % K* maps. The maps were merged using "Multiple-grid-knitting" tools of

Table 1
Statistical parameters of eU, eTh, and % K radio-elements computed for the various geological rock units of the study area.

Age	Rock Units	N	Radio elements	Max.	Min.	Mean (X)	S. D	C.V %
Quaternary	*AL*	8	U (ppm)	2.87	2.81	2.85	0.02	0.72
			Th (ppm)	11.08	11.02	11.05	0.02	0.21
			K (%)	0.75	0.70	0.73	0.02	2.36
Tertiary	*Bb*	12	U (ppm)	3.76	3.71	3.74	0.02	0.46
			Th (ppm)	14.80	14.30	14.55	0.17	1.17
			K (%)	1.35	1.22	1.28	0.04	3.41
Tertiary	*KK*	113	U (ppm)	3.06	2.38	2.74	0.22	7.91
			Th (ppm)	15.34	9.98	11.30	1.70	15.02
			K (%)	0.96	0.25	0.58	0.18	30.30
Cretaceous	*GS*	46	U (ppm)	4.68	2.97	3.88	0.61	15.70
			Th (ppm)	16.14	11.55	13.55	1.73	12.76
			K (%)	0.87	0.29	0.67	0.21	31.68
Cretaceous	*PS*	69	U (ppm)	3.81	2.74	3.12	0.34	10.94
			Th (ppm)	18.38	11.75	13.29	2.12	15.97
			K (%)	3.15	0.49	1.22	0.78	63.75
Cretaceous	*YL*	62	U (ppm)	4.86	3.05	3.36	0.58	17.35
			Th (ppm)	14.92	11.09	12.66	1.24	9.79
			K (%)	3.09	0.96	1.74	0.64	36.96
Cretaceous	*BS*	35	U (ppm)	3.65	2.09	3.06	0.46	14.93
			Th (ppm)	18.79	11.55	14.99	2.50	16.71
			K (%)	3.34	0.81	1.96	0.96	49.12
Jurassic	*JYG*	10	U (ppm)	3.25	3.21	3.23	0.01	0.44
			Th (ppm)	15.66	15.60	15.63	0.02	0.13
			K (%)	1.27	1.23	1.25	0.01	1.13
Pan-African	*OGe*	71	U (ppm)	4.79	3.05	4.15	0.62	15.03
			Th (ppm)	25.76	13.42	17.63	3.67	20.82
			K (%)	4.10	1.23	3.11	1.08	34.63
Pan-African	*OGp*	8	U (ppm)	4.89	3.71	4.23	0.54	12.72
			Th (ppm)	27.08	24.72	25.90	1.18	4.56
			K (%)	4.30	4.10	4.23	0.10	2.38
Pan-African	*Ch*	12	U (ppm)	3.52	2.85	3.19	0.34	10.52
			Th (ppm)	13.48	13.45	13.47	0.02	0.11
			K (%)	4.10	2.98	3.54	0.56	15.82
Precambrian	*bG*	27	U (ppm)	4.79	3.19	4.14	0.68	16.44
			Th (ppm)	24.72	11.69	17.67	5.47	30.97
			K (%)	4.10	2.28	3.11	0.68	21.85
Precambrian	*MG*	9	U (ppm)	4.69	4.64	4.67	0.02	0.37
			Th (ppm)	22.97	22.92	22.95	0.02	0.07
			K (%)	4.08	4.03	4.06	0.02	0.42

Note: X, denotes arithmetic means, max., represents maximum value, min. refers to the minimum value, S.D means standard deviations, N is the total number of spatial points (geographic locations) where the same lithology outcropped, and radiometric measurements were tied to, C.V denotes coefficient of variability, *AL* = alluvium, *bb* = basalts, *KK* = Keri-Keri Formation, *GS* = Gombe sandstones, *PS* = Pindiga Formation, *YL* = Yolde Formation, *BS* = Bima sandstones, *JYG* = ignimbrites, *OGe* = biotite-hornblende granites, *OGp* = porphyritic biotite-hornblende granites, *Ch* = charnokytes, *BG* = granite-gneiss, and *MG* = migmatites – gneiss.

the geosoft software.

The total amount of radioactive heat production obtained through contribution by each of the radio elements (*eU, eTh*, and *% K*) was calculated by using the relation provided by [31] Rybach (1976) as shown below:

$$\mathrm{RHP}\left(\mu W / m^3\right) = \rho(0.0952\ C_u + 0.0256\ C_{Th} + 0.0348\ C_k) \quad (1)$$

where, C_u and, C_{Th} are the concentration of uranium, thorium radioelements which are measured in weight parts per million (ppm). Meanwhile, *% K* is the weight percentage of potassium radio-elements, and ρ is the average dry rock density of the rocks which are measured in g/cm^3.

The significance of the equation (Eq. (1)) is that it enables the estimates of the magnitudes of energy emitted during the decay of the radionuclides of the radioactive elements [10]. The decay process produces alpha, beta and gamma radiation. A physical check on the equation shows variation in RHP contributions among the three main radioelements of *U, Th,* and *K*. The various constants of 0.0952 (uranium), 0.0256 (thorium), and 0.0348 (potassium) shows the dominance of uranium radio elements in terms of RHP contribution, followed by *Th*, and lastly *K* radio-element which provides the least contribution.

The amount of RHP generated over a given geographical location depends on the quantity of *U, Th, and K* contents of the underlying lithology [1,32]. However, the concentrations of these radio-elements varies significantly according to rock type, composition, and its formation mechanism [1]. This implies that the rock density (rock type), the radio-element's composition influences the amount of RHP to be generated. Rock formation processes such as sedimentation, metamorphism, and magmatic differentiation controls the amount of radio-active minerals to be found in a rock, and consequently the amount of RHP to be generated [1]. Granitic rocks tend to records high RHP values due to the high concentration of U, Th, and K formed during the late stage of magmatic differentiation.

Moreover, the concentration of each of the radioelements was obtained from each of the equivalent uranium (*eU*), equivalent thorium (eTh), and the percentage potassium (*% K*) concentration maps produced.

Now, before assigning rock densities to the various rock units found in the study area, the study area was divided into a total of 16 blocks of 30′ by 30′ sizes for easy computation. The various rock types within each block were first identified and recorded. Hence, a total of 13 rock units were identified to be distributed in the whole of the research area (Fig. 1). The rock densities were then assigned to each rock type found within each of the 16 blocks covering the study area. Following standard rock densities published by [33].

Several positions where the same rock type appears on the study area were observed and their coordinates measured. The total number of those points taken across the various locations within the same lithology are represented by letter "N" (Tables 1 and 2) in each of these points, concentration of each of the radio-elements together with their bulk rock densities was taken and used in the computation of RHP values for the entire rock type.

Statistical parameters such as; minimum, maximum, mean (**X**), standard deviations (**S.D**), and coefficient of variability (**C.V**) were calculated for each of the 13 outlined geological units. These parameters were used to further analyse the data. For instance, the **S.D** gives the measure of the dispersion of the data from the computed mean values. This implies that the larger **S.D** values denotes more dispersed data and vice versa. While, the coefficient of variability (**C.V**) is used to monitor the normalization of each of the rock units. It was computed using Equation (2):

$$\mathrm{C.V} = 100(\mathrm{S.D/X}) \quad (2)$$

The RHP map was created from the results of the RHP values computed via Equation (1) (earlier cited) above. The RHP values computed against each of the 13 petrologic units plus the corresponding coordinates for each rock outcrops were prepared and saved in form of Microsoft excel (CSV) file. The CSV data file was subsequently imported into the Oasis montaj (Geosoft) software for the

Table 2
Statistical parameters of the RHP values computed across the various geological units of the study area.

Age (Myr)	Rock Units	N	Average Rock density (g/cm^3)	Max. (μW/m^3)	Min. (μW/m^3)	mean (x) (μW/m^3)	S.D (μW/m^3)	C.V (%)
Quaternary	*AL*	08	1.92	1.12 ± 0.00	1.10 ± 0.00	1.11 ± 0.00	0.00	0.39
Tertiary	*Bb*	12	2.99	2.34 ± 0.12	2.31 ± 0.12	2.32 ± 0.12	0.12	0.51
Tertiary	*KK*	13	2.24	1.59 ± 0.14	1.10 ± 0.14	1.28 ± 0.14	0.14	11.27
Cretaceous	*GS*	46	2.85	2.53 ± 0.28	1.68 ± 0.28	2.11 ± 0.28	0.28	13.08
Cretaceous	*PS*	69	2.40	1.83 ± 0.13	1.45 ± 0.13	1.63 ± 0.13	0.13	8.08
Cretaceous	*YL*	62	2.32	2.02 ± 0.20	1.41 ± 0.20	1.63 ± 0.20	0.20	12.32
Cretaceous	*BS*	35	2.29	2.25 ± 0.29	1.40 ± 0.29	1.74 ± 0.29	0.29	16.83
Jurassic	*JYG*	10	2.61	1.97 ± 0.005	1.96 ± 0.01	1.96 ± 0.01	0.01	0.25
Pan-African	*OGe*	71	2.64	3.30 ± 0.47	1.79 ± 0.47	2.52 ± 0.47	0.47	18.61
Pan-African	*OGp*	08	2.64	3.42 ± 0.07	3.28 ± 0.07	3.35 ± 0.07	0.07	2.13
Pan-African	*Ch*	12	2.64	2.07 ± 0.03	2.00 ± 0.03	2.04 ± 0.03	0.03	1.66
Precambrian	*bG*	27	2.64	3.25 ± 0.57	1.84 ± 0.57	2.52 ± 0.57	0.57	22.52
Precambrian	*MG*	09	2.74	3.22 ± 0.00	3.21 ± 0.00	3.21 ± 0.00	0.00	0.13

Note: X, denotes arithmetic means, max. represents maximum value, min. refers to the minimum value, S.D means standard deviations, N is the total number of spatial points (geographic locations) where the same lithology outcropped, C.V denotes coefficient of variability, *AL* = alluvium, *bb* = basalts, *KK* = Keri-Keri Formation, *GS* = Gombe sandstones, *PS* = Pindiga Formation, *YL* = Yolde Formation, *BS* = Bima sandstones, *JYG* = ignimbrites, *OGe* = biotite-hornblende granites, *OGp* = porphyritic biotite-hornblende granites, *Ch* = charnokytes, *bG* = granite-gneiss, and *MG* = migmatites – gneiss.

continuation of the process of RHP map production. The imported CSV data file was assigned a coordinate system (WGS-84/UTM Zone 32 N). A minimum curvature method of data gridding was applied to the imported data using a grid interval of 100 m. The RHP map was finally created using the earlier gridded file via the use of a 'map tool' in the geosoft environments.

4. Result and discussion

4.1. Statistics of the petrologic units

Certain statistical parameters provide a measure of the central tendency of a population (data). They include; mean, median and mode. However, other parameters such as variance, and standard deviations (S.D) tends to measure the spread or dispersal of the data. For the purpose of this work, statistical parameters such as minimum, maximum, mean, standard deviation, and coefficient of variation (C.V %) were computed for each of the 13 outline lithological units.

The statistical parameters of the individual petrologic units' in terms of *U*, *Th, K* radio-elements abundances analyzed are as presented below; In terms of uranium concentration, the sedimentary petrologies of *AL, KK, GS, PS, YL* and *BS* has an average value of 2.85 ppm, 2.74 ppm, 3.88 ppm, 3.12 ppm, 3.36 ppm, and 3.06 ppm, respectively (Table 1). Gombe sandstone (*GS*) showed the greatest average *U* concentration among sedimentary petrologies examined. The high *U* abundance could be attributed to epigenic process such as migration, and dispersion from the nearby granitic and metamorphic rocks (OGe, OGp, BG etc.). A least value of average *U* concentration of 2.85 ppm is found at the quaternary alluvium (*AL*) rock unit. The average uranium concentration found in the above listed rocks are found to be comparatively higher than the average crustal values of range 2.0 ppm–3.0 ppm earlier reported by [29].

Similarly, in terms of thorium radio-elements distribution among the earlier listed sedimentary petrologies, it could be seen that the rocks have an average *Th* concentration of 11.05 ppm, 11.03 ppm, 13.55 ppm, 13.29 ppm, 12.66 ppm, and 14.99 ppm respectively. The greatest *Th* abundance value recorded was at Bima sandstones (BS) petrologic unit.

A comparison of the average *Th* concentration found among these lithologies showed Gombe sandstones (GS), Pindiga Formation (PS), Yolde Formation (YL), and Bima sandstones to be above the range of 8.0 ppm–12.0 ppm for average crustal rocks [29]. However, Keri-Keri Formation and alluvium deposits have average *Th* concentration that is within the range of the average crustal rocks.

A careful check on the average % K distribution among the earlier listed sedimentary petrologies (*AL, KK, GS, PS, YL,* and *BS*), it showed 0.73% K, 0.58% K, 0.67% K, 1.22% K, 1.74% K, and 1.96% K as the respective average distribution. (Table 1). Moreover, a maximum K abundance value of 1.96% K is recorded along *BS* petrologic unit. A comparison of the average K distributions of the above listed sedimentary rock units showed values for all of the petrologic units to be below the average crustal abundance of 2.0% K to 2.50% K [29]. This indicates depletion of K-feldspars within these Formations.

Details on other statistical parameters of all the sedimentary rock units such as maximum, minimum, standard deviation, and coefficient of variation can be found at Table 1.

The spatial distribution of the three radio-elements of *U*, *Th*, and *K* within the tertiary basaltic outcrops (*bb*) of the study area showed uranium to be in the range of 3.76 ppm–3.71 ppm, with a mean value of 3.74 ppm (Table 1). Similarly, the thorium abundance within the same "***bb***" lithology ranges from 14.80 ppm to 14.30 ppm. An average value of 14.55 ppm was recorded among the various basaltic rock outcrops of the area (Table 1). Uranium is a mobile element, as such, its presence in the basaltic rocks' units could be traced to the older granitic and gneissic rocks found in the study area. The uranium radio-element might have been acquired by the tertiary basalts through epigenetic processes [26].

The migmatites (MG) petrologic unit also depicts *U*, *Th*, and *K* contents that varies from 4.69 ppm to 4.64 ppm, 22.97 ppm–22.92 ppm, and 4.08% K to 4.03% K respectively. The above respective values are however found to be higher when compared to their respective AVC values of 2.0–3.0 ppm, 8.0–12.0 ppm, and 2.0% K–2.50% K [29]. Similarly, the banded gneiss (*bG*) showed range of *U*, *Th*, and *K* values of 4.69 ppm–4.64 ppm, 22.97 ppm–22.92 ppm, and 4.08 *K%*–4.03 *K%* respectively. The above quoted values are comparatively higher than the AVC values of 2.0 ppm–3.0 ppm, 8.0 ppm–12.0 ppm, and 2.0% *K*–2.50% *K* reported by [29].

On a general note, the minimum and maximum values of the average uranium concentration of all the studied rocks are 2.74 ppm, (recorded along *KK*) and 4.67 ppm (recorded along *MG*) respectively. A lowest average thorium concentration of 11.05 ppm is recorded along alluvium deposit (*AL*), while a maximum average value of 25.90 ppm is recorded along OGp rock (Table 1). Furthermore, a lowest average value of 0.58% K was recorded along *KK* Formation. Meanwhile, a maximum average of 4.23% K was observed along *OGp* granites (Table 1).

A careful check on the *U, Th, and K* contents of the other granitic rocks such as *Ch, JYG*, and the remaining two other granites of *OGe*, and *OGp* (Table 1) has shown these granites to be having higher values compared to their respective AVC values as reported by [29].

Therefore, the general analysis of the concentration of the three radio-elements of *U, Th,* and *K* across the 13 petrologic units of the study area showed variable concentration among the petrologic units, spanning from the sedimentary petrologies to the crystalline basement petrologies. Generally, the *U, Th,* and *K* contents of the petrologies examined showed an obviously enhanced signatures compared to their abundance in the crustal rocks. The higher values within the sedimentary petrologies can be explained on the basis of dispersion and migration of these radio-elements from their original sources that are mostly granites [26]. The two prominent granites (*OGe*, and *OGp*) and the metamorphic petrologies (*MG*, and *bG*) are considered as the probable primary sources of these radio-elements. The high contents of these radio-elements found within these set of rocks can be attributed to high ionic radii of these elements. The occurrence of hydrothermal events during the late stage of magmatic crystallization controls their abundance in granites. While, contact metasomatic processes might have caused the higher values found in the two metamorphic units (*MG*, and *bG*) studied.

Based on the magnitudes of abundance of uranium, thorium, and potassium radio-elements, the 13 petrologic units can be re-arranged as below;

- Based on uranium abundance;

  KK < Al < BS < PS < Ch < JYG < YL < bb < GS < bG < OGe < OGp < MG.
  ▶ Increasing order of abundance.

- Based on thorium abundance;

  Al < KK < YL < PS < Ch < GS < bb < BS < JYG < OGe < bG < MG < OGp.
  ▶ Increasing order of abundance.

- Based on potassium abundance;

  KK < GS < Al < PS < JYG < bb < YL < BS < OGe/bG < Ch < MG < OGp.
  ▶ Increasing order of abundance.

An analysis of the RHP generation capacities of the different individual petrologic units is as provided below; The sedimentary rock units such as; alluvium (*AL*), Keri-Keri Formation (*KK*), Gombe sandstones (*GS*), Pindiga Formation (*PS*), Yolde Formation (*YL*), and Bima sandstones (*BS*) shows the range of RHP generation to be; (1.10 $\mu W/m^3$ to 1.12 $\mu W/m^3$), (1.10 $\mu W/m^3$ to 1.59 $\mu W/m^3$), (1.68 $\mu W/m^3$ to 2.53 $\mu W/m^3$), (1.45 $\mu W/m^3$ to 1.83 $\mu W/m^3$), (1.41 $\mu W/m^3$ to 2.02 $\mu W/m^3$), and (1.40 $\mu W/m^3$ to 2.25 $\mu W/m^3$) respectively (Table 2).

However, the overall RHP values recorded among the sedimentary units of the area are found to be in the range of 1.11 $\mu W/m^3$ to 2.11 (Table 2), with an average value of 1.58 $\mu W/m^3$ (Table 3). The average sedimentary value of 1.58 $\mu W/m^3$ obtained in the present study is comparatively higher than the 0.44 $\mu W/m^3$, 0.90 $\mu W/m^3$, and 1.48 $\mu W/m^3$ RHP values reported by [2,22], and [27] as the sedimentary average found within their study localities (Table 3). The sedimentary petrologic unit that displayed the lowest RHP value of 1.11 $\mu W/m^3$ is alluvium sediments While, the maximum RHP value of 2.11 $\mu W/m^3$ recorded within sedimentary petrology is found along the Gombe sandstones outcrops.

The 1.11 $\mu W/m^3$ to 2.11 $\mu W/m^3$ range of values obtained in the present study is slightly higher than the 0.33 to 1.8 0 $\mu W/m^3$ range for the average crustal Sedimentary rocks [24].

The granitic rock units of the study area comprising of the ignimbrites (*JYG*), biotite-hornblende granites (*OGe*), porphyritic biotite granites (*OGp*), and charnokytes (*Ch*) showed the following respective ranges of RHP capacities: JYG (1.95–1.97), OGe (1.79–3.3), OGp (3.28–3.42), and Ch (2.0–2.07) (Table 2). The granitic rocks of the basement complex parts displayed the maximum RHP measurements, whose values ranged from 1.96 $\mu W/m^3$ (along ignimbrites) to 3.35 $\mu W/m^3$ (over porphyritic biotite-hornblende granites).

The average RHP values of 2.5 $\mu W/m^3$ presented for the present granites is comparatively lower than the 3.2 0 $\mu W/m^3$, 3.90 $\mu W/m^3$, 2.94 $\mu W/m^3$, and the 2.60 $\mu W/m^3$ values earlier reported by [1,25,27], and [30] respectively (Table 3). However, the average RHP values of the granitic rocks found in the present research is higher than the average crustal granite value of 1.48 $\mu W/m^3$ [24]. Moreover, the average granitic RHP values obtained in the present study is greater than the 2.40 $\mu W/m^3$, and 2.03 $\mu W/m^3$ values reported for Gebel Duwi, Egyptian granites, and south western Nigerian granites by [24], and [7] respectively (Table 3).

The two prominent metamorphic petrologic units of granite gneiss (*bG*), and migmatites-gneiss (*MG*) has RHP values that ranged from 2.52 $\mu W/m^3$ to 3.21 $\mu W/m^3$, with an average value of 2.87 $\mu W/m^3$ (Table 3). Upon comparison of these values with those

Table 3
Comparison of the present estimated RHP values to those obtained in Nigeria and other parts of the globe.

S/No	Lithology	Location	Average RHP ($\mu W/m^3$)	References
1	Granites	Egypt	3.20	[25]
2	Granites	Egypt	3.90	[1]
3	Basic Igneous rocks	Norway	0.74	[34]
4	Gneissic rocks	NW-Nigeria	2.23	[3]
5	Meta-Sediments	Norway	1.55	[34]
6	Granitic rocks	Norway	2.94	[34]
7	Granites	Australia	2.60	[35]
8	Sedimentary rocks	NW-Nigeria	0.44	[3]
9	Sediments	Australia	0.90	[35]
10	Phosphatic rocks	Syria	1.33	[10]
11	Granites	Gebel Duwi, Egypt	1.48	[24]
12	Basement rocks	SW-Nigeria	2.03	[7]
13	Granites	NE-Nigeria	2.50	present study
14	Sedimentary rocks	NE-Nigeria	1.58	present study
15	Gneisses	NE-Nigeria	2.87	present study
16	Basalts	NE-Nigeria	2.32	present study

obtained in studies by [3], and [34], it can be seen that those from the present research are higher than those from the two previous studies. Moreover, the basaltic rock units of the study area has an average value of 2.32 $\mu W/m^3$ which is higher than the 0.74 $\mu W/m^3$ reported by [34] for the basic rocks of Norway (Table 3).

The general observation of the RHP values when compared with other previous studies such as [2], and [6] who reported RHP values of granites and gneissic rocks (within northwest, and southwestern Nigeria) to be within a range of 0.40 $\mu W{\cdot}m^{-3}$ to 2.34 $\mu W{\cdot}m^{-3}$ and 1.10 $\mu W{\cdot}m^{-3}$ to 1.50 $\mu W{\cdot}m^{-3}$ respectively. This shows that the present result is within the range of their findings.

Furthermore, an examination of the overall radiogenic heat estimates of the petrologic units of the entire study area whose values range from 1.11 $\mu W{\cdot}m^{-3}$ to 3.35 $\mu W{\cdot}m^{-3}$ are found to be comparatively lower than the threshold value of 4.0 $\mu W/m^3$. The 4 .0 $\mu W/m^3$ value is considered to be the minimum limit for moderate RHP generation by lithologies [3,36]. Hence, on the basis of the above global classification, the RHP of the present petrologic units reported can be said to be low in terms of geothermal character. The 13 petrologic units of the study area can be arranged in the order of decreasing magnitude of RHP generation as enumerated below;

OGp > MG > OGe/bG > bb > GS > Ch > JYG > BS > PS/YL > KK > AL.

▶ Decreasing order of abundance of RHP across the 13 petrologic units.

The overall observation of the pattern of heat production for the area shows high degree of correlation with the geological set up of the area. This can be proved by the display of high heat production from the regions of basements (granitic and gneissic rocks) exposures, whereas, other areas of sedimentary rocks maintain low to moderate heat production.

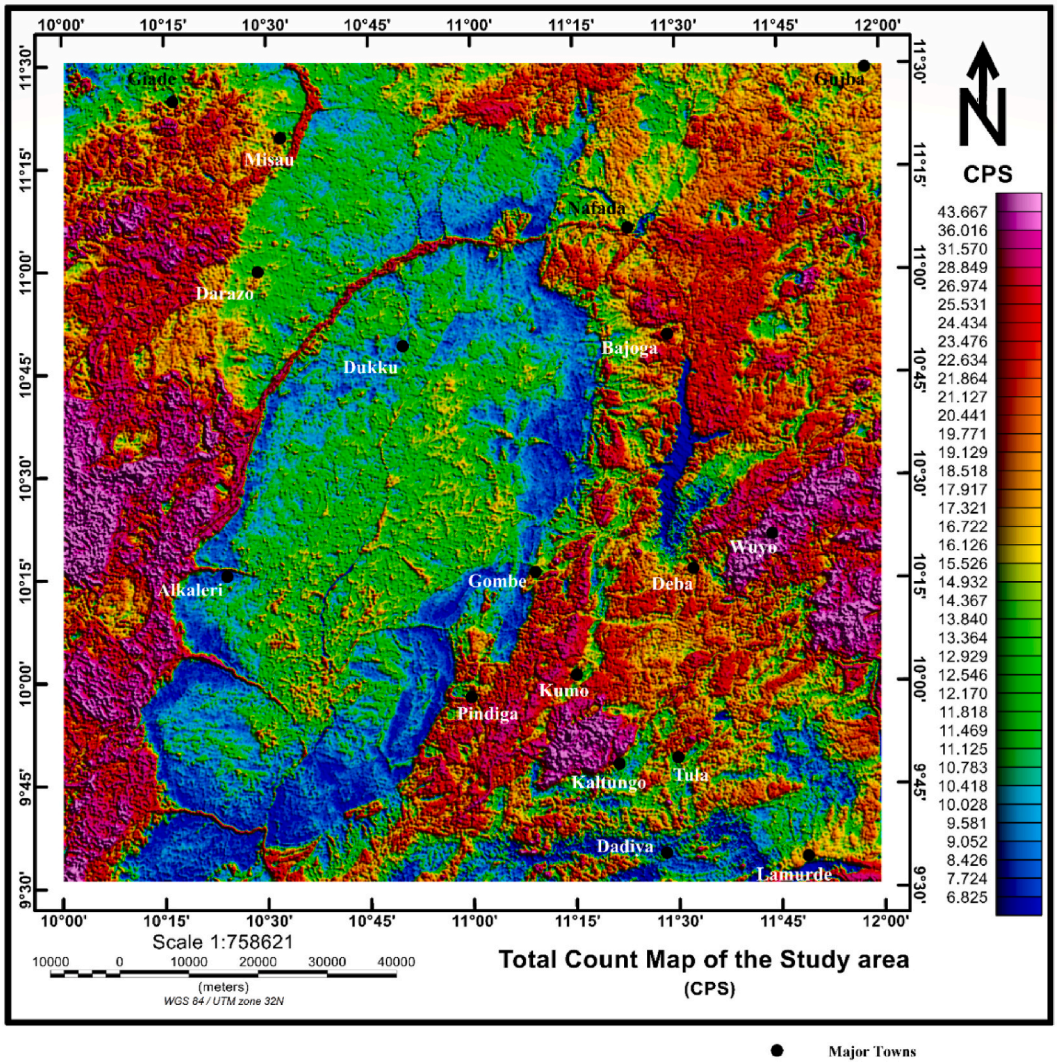

Fig. 3. Total count (cps) map of the study area.

4.2. Total count map

A total count (**TC**) map is a map that reveals the combined measure of the radiometric counts coming from the three main radio-elements of ^{238}U, ^{232}Th, and ^{40}K. The total counts map of the present study area (Fig. 3) has a maximum value of 43.67 cps and a minimum of 6.83 cps. A total count map of an area helps in geological mapping of an area, as it shows the composite radiometric effects of *U, Th,* and *K* elements in every rock unit outcropping in an area.

A careful study of Fig. 3 shows the preponderance of high values of TC (reddish – magenta colours) along the granitic rock's exposures of the study area. Other areas exhibiting moderate total counts measurements (yellow – reddish coloured) corresponds with either the mafic igneous rock outcrops or other sedimentary rocks that includes; Bima formation, Yolde formation, Pindiga formation and Gombe formation. The map further discloses some regions that exhibits lower total counts measurements (blue-greenish coloured). The Keri-Keri formation found at the central parts of the study area exhibits this kind of low total counts values.

A colour composite radio-element (ternary) image map (Fig. 4) was used to display the various radio-elements compositions within the different rock distributions of the study area. Three colours of red, blue, and green were assigned to *eU, eTh,* and *% K respectively*. The colours of the triangular shape legend (Fig. 4) also corresponds to the red, blue, and green colours assigned to *eU, eTh,* and *% K* earlier on. The 100% values indicated at each of the three ends of the triangle indicates the maximum value (absolute concentration) of each of the radio-elements represented by the colours displayed in the map.

4.2.1. Equivalent uranium (^{238}U) concentration map

Equivalent uranium (*eU*) concentration map (Fig. 5) portrays three-four levels of concentration of uranium. These include; the magenta-coloured anomalies that ranges from 4.60 ppm to 6.0 ppm. These very high uranium concentration areas correlate with the granites and gneissic rocks out crops at the western parts of the studied area (near Alkaleri, Darazo, and Misau towns). Other areas with high uranium concentration anomalies include; the central parts of Fig. 5 (near Bajoga, Kumo, Pindiga and Kaltungo areas). Moreover, the extreme north (near Nafada town), and extreme east of the map also displayed high level of *U* concentrations (Fig. 5). Certain aspects of Fig. 5 show moderate - high level of uranium concentration. These are yellowish to reddish coloured anomalies that ranges from 2.80 ppm–4.40 ppm. Some of the moderate – high anomalous features stretch from Gombe, to Dukku, and Misau areas (Fig. 5). On the contrary, some locations show very low to low uranium concentration levels. They are the blue wish-greenish coloured

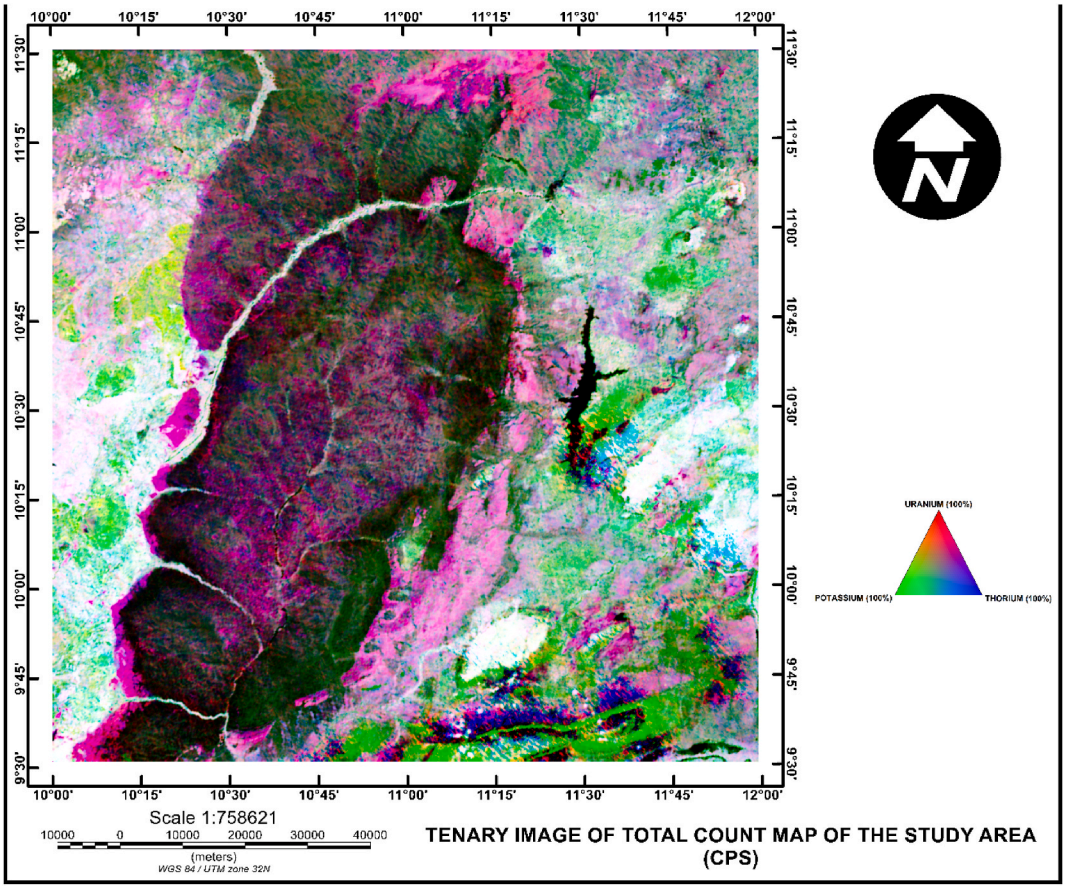

Fig. 4. Ternary image of the total count map of the study area.

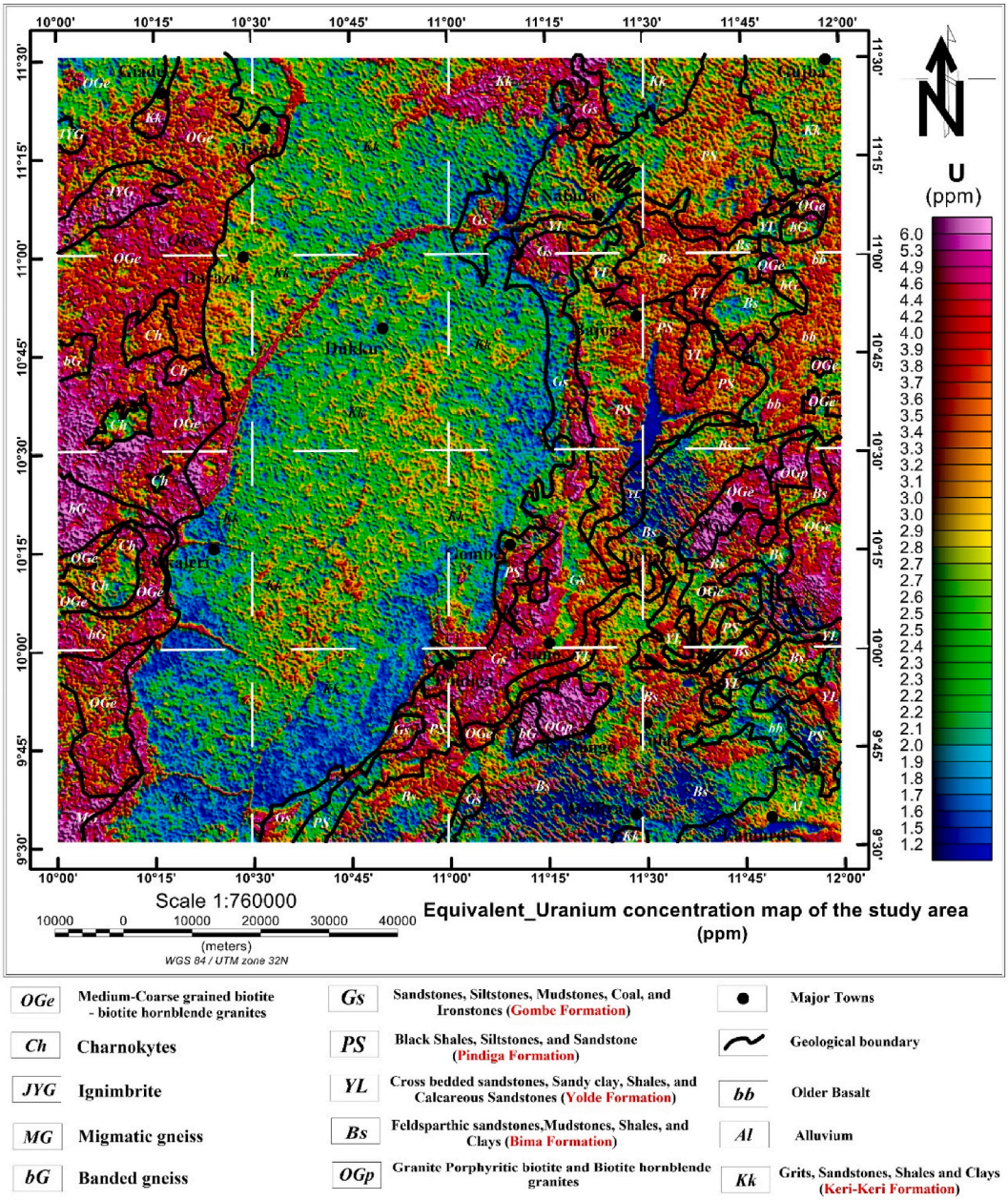

Fig. 5. Equivalent uranium (*eU*) concentration map of the study area (in ppm) with geology map overlaid on it.

anomalies. These areas have uranium concentration that ranges from 1.20 ppm to 2.70 ppm, and are found to be located around Gombe areas, northern, and eastern parts.

4.2.2. *Equivalent thorium (^{232}Th) concentration map*

The equivalent thorium concentration map (Fig. 6) of the study area shows areas with the greatest level of thorium content (20.50 ppm–34.50 ppm) to be represented by the magenta coloured anomalies, and are found to be located near Wuyo, Kaltungo, Pindiga, and Kumo towns. Other areas that depict high thorium contents includes; the western parts of the map near Alkaleri, Darazo, and Misau towns.

Furthermore, the overall equivalent thorium concentration of the study area ranges from 5.10 ppm to 34.50 ppm. Locations that portray moderate to high level of thorium are represented by the yellowish to reddish coloured anomalies that range from 11.30 ppm–20.50 ppm. These areas are the second largest in terms of areal coverage after the blue - greenish coloured part. They showed a very low to low concentration of Thorium radio-elements (5.10 ppm–11.70 ppm).

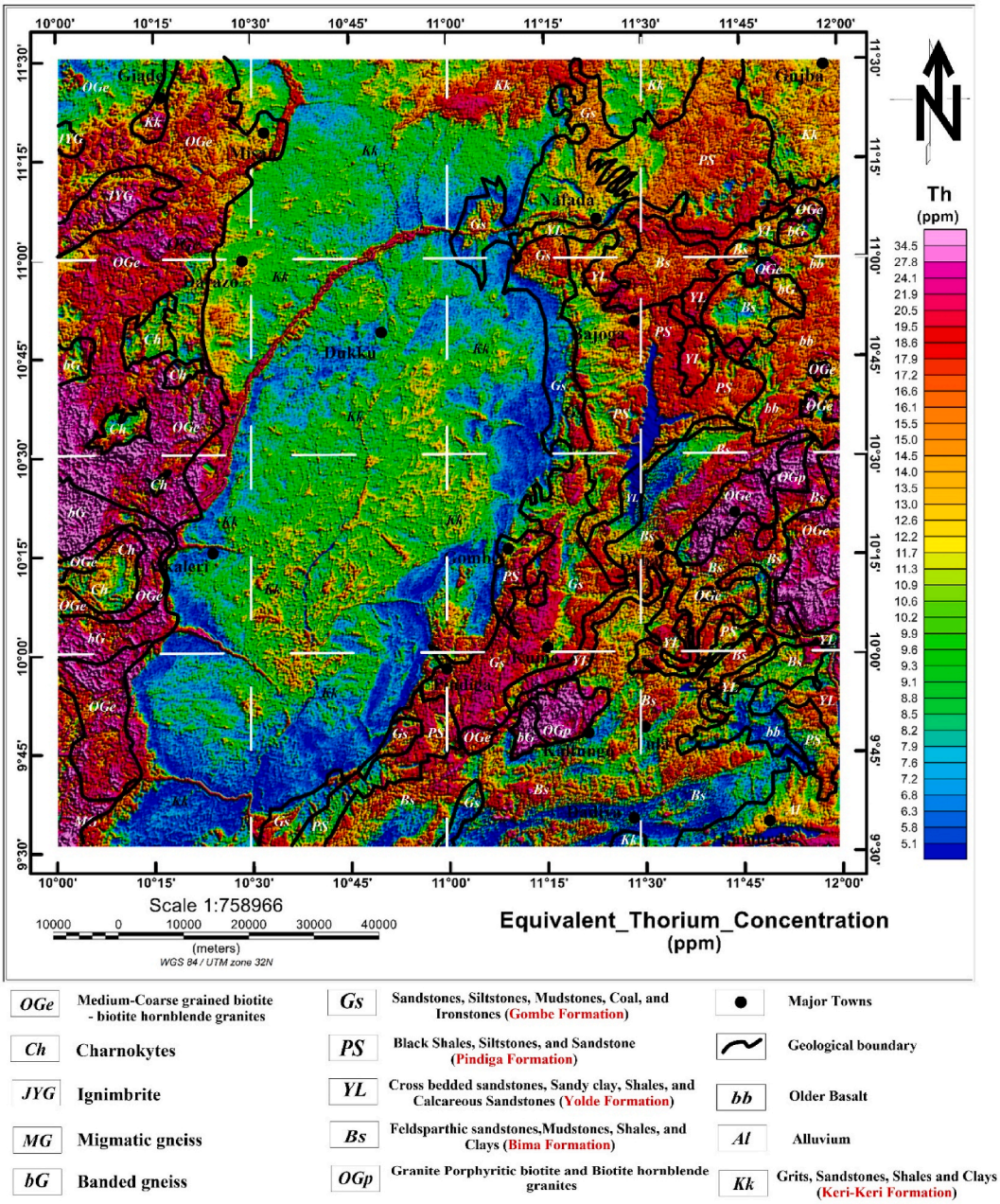

Fig. 6. Equivalent thorium (*eTh*) concentration map of the study area (in ppm) with geology map overlaid on it.

4.2.3. Percentage potassium (^{40}K) concentration map

Fig. 7c shows the variation of potassium (^{40}K) concentration over the study area. It also shows three main locations of prominent (very-high) concentration of potassium content. These locations are represented by the pinkish coloured anomalies that ranged from 3.50% K to 4.70% K (also labelled as: **U**, **V**, **W**, **X**, and **Y**) (Fig. 7c). Areas depicting moderate to high % *K* values (yellowish to reddish coloured anomalies), ranges from 0.60% K to 3.50% K and are labelled as; **M**, **N**, **O**, **P**, and **Q**. The Blue to greenish coloured anomalies represents areas that portrays low to very low (0.10% K–0.60% K % values) contents of potassium. This anomaly occupied the largest segment of the total areal coverage of the map.

4.3. Radiogenic heat production (RHP) map

The spatial distribution of RHP over the study area is presented in form of a map. The radiogenically produced heat production map generated for the study area (Fig. 8) shows different areas producing different levels of heat. The heat produced can be seen to depict

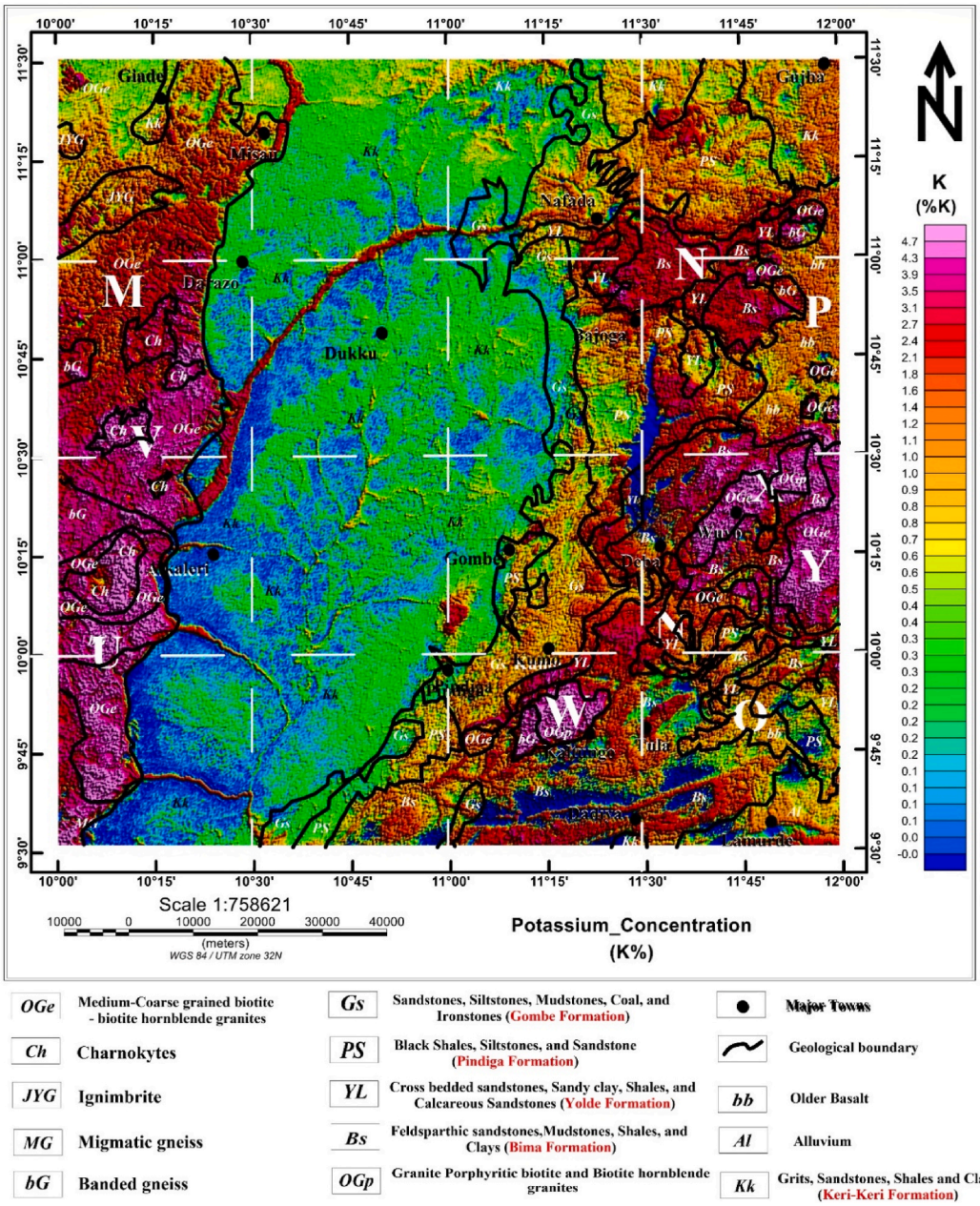

Fig. 7. Percentage potassium (*% K*) concentration map of the study area with geology map overlaid on it.

variable level of radiation. Basically, there are four (4) levels of radiation in the RHP map. The high-level radiogenic heat production areas have the heat production range of 2.0 $\mu W/m^3$ to 2.90 $\mu W/m^3$. These are represented by reddish to magenta-coloured anomalies (Fig. 8). There are seven prominent anomalies that exhibits high heat emission from the RHP map. These anomalies are labelled from **A** to **F**. These anomalies are displayed in different parts of the RHP map (Fig. 8). The radiometric high heat production zones correspond to the basements (granitic, gneissic) rocks, as well as the basic rocks outcrops of the western and eastern parts of the map (Fig. 8). This phenomenon can be explained on the basis of the fact that usually, the granitic rocks tend to have high content of *U, Th, and K* radio-elements compared to their sedimentary counterparts, which could further be related to their formation modes. The amount of radiometric heat production by a given rock is dependent on the type of rock involved, which also depends on the mineralogical content of the rock [24].

Further examination of the RHP map (Fig. 8) shows the moderate RHP zones to be exhibiting the RHP value of 1.70 $\mu W/m^3$ – 2.0 $\mu W/m^3$. These are represented by the greenish - yellowish coloured anomaly labelled **M**.

Other regions show moderate levels of radiogenic heat production in the map. These are denoted by the yellowish to greenish

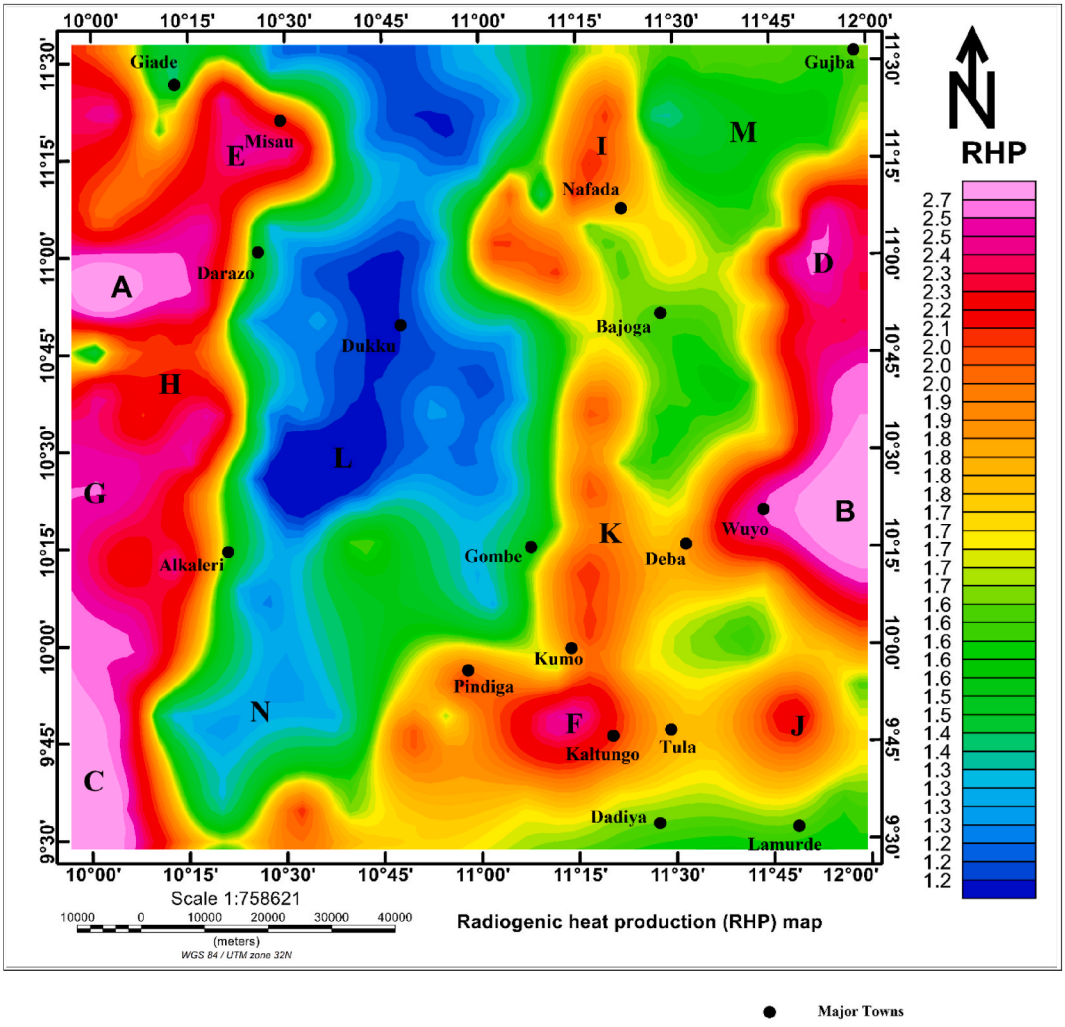

Fig. 8. Radiogenically produced heat (RHP) map of the study area (measured in $\mu W/m^3$).

coloured anomalies found at both western and eastern parts of the RHP map. They are labelled with letter **M**. Some of these areas of intermediate/moderate heat production were observed to be at the boundary between the basements and the surrounding sedimentary rock outcrops. For instance, an interphase (contact) between the two main rock units. However, anomaly **B** and **D** are found to extend from the sedimentary rock outcrops (Bima formation, Yolde formation) to the location of the Lunguda basalts at the south eastern parts of the map.

The low-level heat production areas (1.40 $\mu W/m^3$ – 1.70 $\mu W/m^3$) corresponds almost entirely with the sedimentary rock outcrops of Keri-Keri formation (*KK*), which is located at the central part of the study area (Fig. 8).

The fourth level of radiogenic emission observed is the very low-level radiation components that is represented by the light blue to dark blue-coloured anomalies (1.40 $\mu W/m^3$ – 1.70 $\mu W/m^3$)

Furthermore, the high radiogenic heat production zone labelled **A,** and **B** shows an agreement with the earlier findings by [12–14,16,18–20,22,23] who used geological, and geochemical approach around; Wuyo, Zona, Mika, Kanawa, and Gubrunde areas to show the occurrence and structural control of uranium mineralization. Therefore, areas labelled **A**, and **B**, around the western and eastern parts of Alkaleri, and Wuyo towns respectively are considered as a highly prospective locations in term of radiometric heat production, as their heat production exceeds the minimum heat production value of 2.40 $\mu W/m^3$ for average crustal granites [24].

5. Conclusion

The present study has provided an insight on the distribution patterns of RHP across the various petrologic units of northeastern Nigeria based on the interpretation of the new high resolution airborne radiometric data over the entire Gongola basin and its environs.

The minimum RHP values of 1.11 $\mu W\ m^{-3}$ correlates with the tertiary alluvium rock deposits of the studied area. While, a maximum RHP average value of 3.35 $\mu W{\cdot}m^{-3}$ falls below the lowest average threshold value of 4.0 $\mu W/m^3$ for geothermal producing

lithologies. But, maximum RHP values of 3.35 $\mu W \cdot m^{-3}$ presented in the present study is within the range of 1.10 $\mu W \cdot m^{-3}$ to 1.50 $\mu W \cdot m^{-3}$ (for younger granites) and 0.40 $\mu W \cdot m^{-3}$ to 2.34 $\mu W \cdot m^{-3}$ (for gneissic rocks) reported by [3].

The aero radiometric data used helped in computing the previously non available radiogenic heat production (RHP) map of the studied area.

The studied petrologic units showed variable level of ^{238}U, ^{232}Th, and ^{40}K, radioelements distribution. The average *U, Th,* and *K* concentrations are in the range of 2.74 ppm–4.82 ppm, 11.05 ppm–25.90 ppm, and 0.58% K–4.20% K respectively. Interns of RHP correlation with their corresponding ^{238}U, ^{232}Th, and ^{40}K, radioelements abundance across the entire petrologic units, a greater level of correlation was found, with the greatest level of correlation found with the uranium radioelements.

The correlation of the high RHP measurements with higher abundance radioelements can be attributed to the compositions, and formation mechanism of the geological units.

Seven prominent areas (labelled **A**, to **F**) at different parts of the studied area are considered as highly prospective. As such, they are recommended for further investigation.

Author contributions statement

Abubakar Yusuf, Lim Hwee San, and Ismail Ahmad Abir: Conceived and designed the experiments; Performed the experiments; Analyzed and interpreted the data; Contributed reagents, materials, analysis tools or data; Wrote the paper.

Funding statement

This research received funding from Tertiary Education Trust (TET) Fund, Nigeria, and 'Fundamental Research Grant Scheme' (FRGS/1/2021/STG08/USM/02/2) from the Ministry of Higher Education, Malaysia.

Data availability

The data will be made available based on request.

Additional information

There is no available additional information.

Declaration of competing interest

The authors declare that they have no known competing financial interests or personal relationships that could have appeared to influence the work reported in this paper.

Acknowledgements

The authors are grateful to Universiti Sains MalaysiaUniversiti Sains Malaysia (USM) for providing financial support through the '*Fundamental Research Grant Scheme*' (*FRGS/1/2021/STG08/USM/02/2*), with account code; *FGRS 203.PFIZIK.6712011* from the Ministry of Higher Education Malaysia.

Special appreciation goes to *Tertiary Education Trust (TET) Fund*, Nigeria for the financial support given to the first author of this paper.

References

[1] A.A. Adel, G.E. Abbady, A.M. El-Arabi, Heat production rate from radioactive elements in igneous and metamorphic rocks in Eastern Desert, Egypt, Appl. Radiat. Isot. 64 (2006) (2006) 131–137, https://doi.org/10.1016/j.apradiso.2005.05.054.

[2] A.G.E. Abbady, Evaluation of heat generation by radioactive decay of sedimentary rocks in Eastern Desert and Nile Valley, Egypt, Appl. Radiat. Isot. 68 (2010) (2010) 2020–2024, https://doi.org/10.1016/j.apradiso.2010.03.023.

[3] J. Aisabokhae, Adeoye Moses, Spatial distribution of radiogenic heat in the Iullemmeden basin – precambrian basement transition zone, NW Nigeria, Geol. Geophys. Environ. 46 (3) (2020) 239–250.

[4] M. Pleitavino, M.E.C. Pérez, E.G. Aráoz, M.A. Cioccale, Radiogenic heat production in granitoids from the Sierras de Córdoba, Argentina, Geoth. Energy (2021), https://doi.org/10.1186/s40517-021-00198-9.

[5] A. Yusuf, A.I.A. San, Hwee Lim, A preliminary geothermal prospectivity mapping based on integrated GIS, remote-sensing, and geophysical techniques around northeastern Nigeria, Sustainability 13 (2021) 8525.

[6] J. Wilford, Airborne gamma-ray spectrometry, AGSO J. Aust. Geol. Geophys. (January 2002) (2014).

[7] A.S. Akingboye, A.C. Ogunyele, T.A. Jimoh, B.O. Adaramoye, O.A. Adeola, T. Ajayi, Radioactivity, radiogenic heat production and environmental radiation risk of the basement complex rocks of Akungba - Akoko, southwestern Nigeria: insights from in situ gamma - ray spectrometry, Environ. Earth Sci. 80 (2021) 1–24.

[8] A. Elkhadragy, M.S.A. Ali, A.G.N. Gharieb, A.A. El-husseiny, The use of airborne spectrometric data in geological mapping and uranium exploration at Qena-Quseir shear zone area, eastern desert, Egypt, Glob. J. Sci. Front. Res. H Environ. Earth Sci. 16 (5) (2016) 29–48.

[9] J. Asfahani, M. Aissa, R. Al-Hent, Evaluation of radioactive environmental hazards in area-3, Northern Palmyrides, Central Syria using airborne spectrometric gamma technique, Appl. Radiat. Isot. 107 (2016) 259–271, https://doi.org/10.1016/j.apradiso.2015.10.029.

[10] J. Asfahani, Estimation and mapping of radioactive heat production by aerial spectrometric gamma and fractal modeling techniques in the Syrian desert (Area-1), Syria, Appl. Radiat. Isot. (2018), https://doi.org/10.1016/j.apradiso.2018.09.004.

[11] A.L. Sabra, M. Mohamed Elsadek, Abdeldayem, M.A.S. Youssef, A.A. Masoud, S.A. Mansour, Determination of the radiation dose rate and radiogenic heat production of North Gabal Abu Hibban area, central Eastern Desert, Egypt, NRIAG J. Astron. Geophys. 8 (1) (2019) 103–111, https://doi.org/10.1080/20909977.2019.1617556.
[12] I.O. Oshin, M.A. Rahaman, Uranium favourability study in Nigeria, J. Afr. Earth Sci. 5 (2) (1986) 167–175.
[13] I. Dada, S.S. Tusosun, J. Lancelot, A. Lar, Late Archaean U-Pb age for the reactivated basement of Northeastern Nigeria, J. Afr. Earth Sci. 16 (4) (1993) 405–412.
[14] A.T. Bolarinwa, S. Bute Ibrahim, Petrochemical and tectonogenesis of granitoids in the Wuyo-Gubrunde petrochemical and tectonogenesis of granitoids in the Wuyo-Gubrunde Horst, northeastern Nigeria: implication for uranium enrichment, Nat. Resour. Res. 25 (2) (2016) 197–210, https://doi.org/10.1007/s11053-015-9279-7.
[15] S.I. Bute, X. Yang, J. Cao, L. Liu, J. Deng, I.V. Haruna, M.B. Girei, U. Abubakar, S. Akhtar, Origin and tectonic implications of ferroan alkali- calcic granitoids from the Hawal Massif, east- eastern Nigeria terrane: clues from geochemistry and zircon U-Pb-Hf isotopes, Int. Geol. Rev. 62 (2) (2020) 129–152, https://doi.org/10.1080/00206814.2019.1593250.
[16] C.E. Suh, S.S. Dada, Fault rocks and differential reactivity of minerals in the Kanawa Violaine uraniferous vein, NE Nigeria, J. Struct. Geol. 19 (8) (1997) 1037–1997.
[17] C.E. Suh, S.S. Dada, T.R. Ajayi, G. Matheis, Integrated structural and mineral alteration study of the Zona uranium anomaly, northeast Nigeria, J. Afr. Earth Sci. 27 (1) (1998) 129–140, https://doi.org/10.1016/S0899-5362(98)00051-7.
[18] S.S. Suh, CE, Dada, Mesostructural and microstructural evidences for a two stage tectono-metallogenetic model for the uranium deposit at Mika, northeastern Nigeria: a research note, Nonrenewable Resour. 7 (1) (1998) 75–83.
[19] I. V Haruna, H.A. Ahmed, A.S. Ahmed, Geology and tectono-sedimentary disposition of the Bima sandstone of the upper benue trough (Nigeria): implications for sandstone-hosted uranium deposits, J. Geol. Min. Res. 4 (December) (2012) 168–173, https://doi.org/10.5897/JGMR12.008.
[20] I.V. Haruna, Lithologic features and uranium possibilities of the granites of Pupule, Adamawa massif N.E. Nigeria, Global J. Geol. Sci. 15 (2017) 57–64.
[21] I.A. Haruna, D.P. Ameh, A.A. Mohammed, U. Umar, Uranium mineralization in Gubrunde Horst, upper benue trough, north-east, Nigeria, J. Geosci. Geomatics 5 (3) (2017) 136–146, https://doi.org/10.12691/jgg-5-3-5.
[22] S.I. Bute, Uranium ore deposit in northeastern Nigeria: geology and prospect, Continent. J. Earth Sci. 8 (January 2013) (2013) 21–28, https://doi.org/10.5707/cjearthsci.2013.8.1.21.28.
[23] S.I. Bute, Petrography, geochemistry and alteration studies of Kanawa uranium, J. Geol. Geophys. 6 (4) (2017) 4–11, https://doi.org/10.4172/2381-8719.1000297.
[24] A. Salem, A. Elsirafy, A. Aref, A. Ismail, S. Ehara, K. Ushijima, Mapping radioactive heat production from airborne spectral gamma-ray data of Gebel Duwi area, Egypt, Proceedings World Geothermal Congress 2005 (April) (2005) 24–29.
[25] A.G.E. Abbady, A.H. Al-ghamdi, Heat production rate from radioactive elements of granite rocks in north and southeastern Arabian shield Kingdom of Saudi Arabia, J. Radiat. Res. Appl. Sci. (2018) 1–10, https://doi.org/10.1016/j.jrras.2018.03.002.
[26] A.A. Adepelumi, A.H. Falade, Combined high-resolution aeromagnetic and radiometric mapping of uranium mineralization and tectonic settings in Northeastern Nigeria, Acta Geophys. (2017), https://doi.org/10.1007/s11600-017-0080-3.
[27] N.G. Obaje, Geology and Mineral Resources of Nigeria, 2009.
[28] A.U. Shettima, I.Y. Buba, M.W. Sidi, Y. Abdulganiyu, H. Hamidu, Reservoir potentials of the cretaceous Gombe sandstone, Gongola basin, upper benue trough, north eastern Nigeria, J. Appl. Geol. Geophys. 4 (July) (2016) 66–77, https://doi.org/10.9790/0990-0404026677.
[29] S. Erdi-Krausz, M. Matolin, B. Minty, J.P. Nicolet, W.S. Reford, Guidelines for radioelement mapping using gamma ray spectrometry data, Geophysics (July) (2003) 1–152.
[30] Nigerian Geological Survey Agency (NGSA), Airborne Geophysical Digital Data Dissemination Guidelines, 2010, pp. 1–24.
[31] B.L. Rybach, Radioactive heat production in rocks and its relation to other petrophysical parameters 1), Pure Appl. Geophys. 114 (111) (1976).
[32] K.S. Din, Estimation of heat generation by radioactive decay of some phosphate rocks in Egypt, Appl. Radiat. Isot. 67 (11) (2009) 2033–2036, https://doi.org/10.1016/j.apradiso.2008.10.016.
[33] S.L.P. Telford, WM, R.E. Geldart, Appl. Geophys. 127 (3212) (1990).
[34] T. Slagstad, Radiogenic heat production of Archaean to Permian geological provinces in Norway, Nor. J. Geol. 88 (3) (2008) 149–166.
[35] M.F. Middleton, Radiogenic heat generation in western Australia — implications for geothermal energy, Adv. Geotherm. Energy (2016) 49–90.
[36] D.L. Huston, An Assessment of the Uranium and Geothermal Potential of North Queensland, 2010.